Time-Domain Oscillographic Microwave Network Analysis Using Frequency-Domain Data

MARION E. HINES, FELLOW, IEEE, AND HAROLD E. STINEHELFER, SR., SENIOR MEMBER, IEEE

Abstract—**Oscillographic plots of various time-domain responses of microwave networks are generated by computer simulation, based upon measurements taken in the frequency domain. Frequency-response data are obtained with a computer-controlled automatic network analyzer, this information is processed in an associated computer, and selected time-domain responses are plotted immediately on an x–y recorder. Voltage versus time responses have been simulated for various excitations including impulse, step, and pulse-modulated RF waves. When impedance data are used, the plots are interpretable as from a time-domain reflectometer with high precision, high sensitivity, and high resolving power. As an oscillograph the rise time may be as short as 0.04 ns. In transmission 70 dB or more loss can be tolerated. In reflection measurements, the results are interpretable for discrete discontinuities with 40 dB or more return loss, and with separations on the order of 1 cm in space.**

In certain types of circuits, time-domain data can be used to reconstruct the frequency-domain response data in an approximate manner for separate parts of a network without separate measurements. In this manner, the interference of generator, load, and transducer mismatches can be substantially reduced.

I. Introduction

IT IS WELL KNOWN that specific time-domain responses of a linear network can be predicted theoretically if its frequency-response characteristics are fully known. Fourier series transformations are commonly used for such determinations. With the advent of the modern computer-controlled network analyzer, it has become possible to measure the frequency response of networks from essentially zero frequency–18 GHz, at a large number of frequencies in a short time, and to store the data for further computer processing. Using an associated computer and an x–y recorder, a program has been prepared which performs the necessary transformations so that a graph can be immediately drawn which simulates an oscillographic display of the network's response, in time, to various standard input excitations.

In our work, we have used the impulse response, the step response, and an RF pulse. We have found that the resulting instrument is highly precise and the curves may be interpreted quantitatively. The sensitivity is also great, allowing the measurement of highly lossy networks and the resolution of transmission-line discontinuities with a high return loss. As an oscillograph, a rise time of $\sim$40 ps has been observed.

Manuscript received July 19, 1973; revised October 30, 1973.
The authors are with Microwave Associates, Inc., Burlington, Mass. 01803.

In our laboratory we have used a Hewlett-Packard model 8542B Automatic Network Analyzer, a Hewlett-Packard model 9600E Data Acquisition RTE System, and a Hewlett-Packard model 7210A Digital x–y Recorder. Typically, 81 frequency points can be measured at adjacent harmonically related frequencies, which allows a somewhat detailed graph to be drawn over an extended time interval.

The Fourier series approach is well known and straightforward. A standard periodic input waveform is assumed, repetitive at a relatively low "fundamental" frequency. Network measurements are taken at integer harmonics of this fundamental. The input wave function is "shaped" to accomodate the frequency range of the measurements by simulating the effect of a Gaussian "roll-off" filter, and the resultant waveform is resolved into its harmonic spectral components. Each component is modified according to the response of the network at that frequency. The resultant set of frequency components are then summed to obtain the output time function.

Here we have made use of modern computer technology and automatic measuring equipment to generate and process large amounts of data, which in the past required too much labor for ordinary laboratory application.

To simulate an impulse response, the input time function starts as a periodic sequence of δ functions, but is modified by the Gaussian roll-off filter which effectively modifies the pulse shape into that of a sequence of Gaussian pulses of finite width.

For the step response, an input square wave is similarly modified; the Gaussian filter effectively rounding off the leading and trailing edge discontinuities, providing a finite rise time and fall time with little overshoot. In the case of the RF pulse, we begin with ideal δ functions, but a bandpass Gaussian filter is simulated which has the effect of generating a sequence of short RF pulses with a Gaussian envelope. In each case, these input spectral components are subsequently modified by the network response and summed to obtain the simulated output waveform.

In our laboratory, we have found that a major application is its use as a *time-domain reflectometer* for diagnostic study of wide bandwidth transmission networks. In this mode of use, input impedance measurements are taken, converted into reflection coefficient form, and stored. After subsequent time-domain transformation, the oscillographic curve represents the reflected waveform which

would result from excitation of the network by a sequence of widely spaced short Gaussian pulses. From any reflective discontinuity within the network, an equivalent short pulse would be returned to the input, delayed in time by the round-trip path length involved. In the graphs produced by this technique, the effects of small discrete discontinuities are easily discernable, in single or multiple form, with their locations resolvable within a fraction of a centimeter. The character and magnitude of the discontinuities are interpretable in terms of the magnitude and shape of the reflected pulses observed. The effects observed are similar to what one would expect from a radar with a transmitter pulse of spatial length shorter than 1 cm, and an oscillographic display of equivalent rise and fall times. Under some circumstances, reflection points with return loss greater than 40 dB have been resolved.

We have also found the technique useful in obtaining the *frequency response* of the reflection coefficient of one part of a network which is separated by short line lengths from other parts of the network which also cause reflections on the input line. For example, an imperfect uncalibrated transducer may lie between the measuring equipment and the network of interest, and it is desired to eliminate the perturbing effects of this transducer. We have found that the time-domain responses of various parts of a network sometimes can be separated in this way. If now all but one part is ignored, a transformation can be used in reverse to reconstruct the frequency-domain data of that part with little interference from the others. The technique is useful but is subject to errors due to multiple reflections, and from loss of data due to suppression of parts of the plot.

Applications of Fourier series principles to time-domain reflectometry in recent years include an elegant technique of Hollway [1] and Somlo [2] who used specialized equipment with external data processing. Robinson *et al.* [3] describe an approach which is very similar to ours for radar echo studies of objects in space. Nicolson *et al.* [4] describe highly advanced techniques for direct oscillographic study of transmission and reflection of very short pulses. A time-domain reflectometer as a commercial instrument (HP-1818A) is available for direct oscillographic display of reflective waves from networks using a repetitive step-function input wave. Our technique has a time resolution comparable to these other approaches. Its sensitivity for measuring weak reflections is comparable to the techniques of [1]–[3], being similarly limited by interfering reflections from the microwave instrumentation, and from adjacent reflections in the device being studied. Our approach offers a significant advantage in signal to noise and jitter, compared to the direct oscillographic techniques. There is an additional advantage of versatility in that the response to many different waveforms may be simulated with ease, both in transmission and reflection. A still further advantage is that the curves are directly interpretable, quantitatively, without the zero-level drift and zero ambiguity of the sampling oscillograph.

II. Mathematical Basis

Ideally, a Fourier series involves an infinite number of terms. The equations below are useful to represent a continuous or discontinuous voltage waveform $V_i(t)$ of a periodic nature, of period T s:

$$V_i(t) = \frac{V_{co}}{2} + \sum_{n=1}^{\infty} \left[V_{cn} \cos \frac{2\pi nt}{T} + V_{sn} \sin \frac{2\pi nt}{T} \right] \quad (1)$$

$$V_{cn} = \frac{2}{T} \int_{-(T/2)}^{T/2} V_i(t) \cos \frac{2\pi nt}{T} \, dt \quad (2)$$

$$V_{sn} = \frac{2}{T} \int_{-(T/2)}^{T/2} V_i(t) \sin \frac{2\pi nt}{T} \, dt. \quad (3)$$

In (1), an *input* waveform $V_i(t)$ is presented as the sum of an infinite series of sines and cosines of harmonically related frequencies. The harmonic voltages V_{cn} and V_{sn} are determinable by the integrations of (2) and (3). This wave is *periodic*, repeating after an interval of T s with a fundamental frequency $f_1 = 1/T$ Hz. Each frequency term in (1) is an integer harmonic of f_1 at various frequencies nf_1, $0 \leq n < \infty$.

To determine the time-domain response of an electrical network to an arbitrary input waveform $V_i(t)$, we first determine its Fourier series coefficients V_{cn} and V_{sn} using (2) and (3). Equation (1) indices that the input wave consists of a sum of a set of sine and cosine voltage waves of an infinite number of frequencies, each an integer harmonic of the fundamental, the nth harmonic having a frequency $nf_1 = n/T$ Hz. In a linear network there is no interaction between different applied frequencies so that we can linearly superpose the effects of many simultaneous inputs of different frequencies. Therefore, if we determine the complex voltage-response ratio S_n of the network for each harmonic frequency nf_1, we can obtain the *response* set of harmonic voltages and add the result to obtain the time function of the output wave. If

$$S_n = \hat{S}_n \exp j\theta_n \quad (4)$$

where $\hat{S}_n$ is the magnitude of S_n, then the two nth terms of the output Fourier series become

$$V_{on} = \hat{S}_n \left\{ V_{cn} \cos \left(\frac{2\pi nt}{T} + \theta_n \right) + V_{sn} \sin \left(\frac{2\pi nt}{T} + \theta_n \right) \right\} \quad (5)$$

and the total output response waveform becomes

$$V_o(t) = \frac{V_{co}}{2} S_o + \sum_{n=1}^{\infty} \hat{S}_n \left[V_{cn} \cos \left(\frac{2\pi nt}{T} + \theta_n \right) + V_{sn} \sin \left(\frac{2\pi nt}{T} + \theta_n \right) \right]. \quad (6)$$

(Note that the dc response S_0 is always real but may be positive, negative, or zero.)

Infinite series cannot be summed in a computer. We can deal only with a finite number of harmonics, typically 81 in the present system, where we have a usable frequency range from ~ 110 MHz to 18 GHz. When a Fourier series for a discontinuous waveform is truncated after a finite number of terms, the reconstructed wave shows overshoots and ringing transients preceding and following each discontinuity. Pulse shaping is a well-known practice for reducing such effects, and has been used for many years in pulse systems. Various methods are known. Here we have simulated the effect of a pulse-shaping filter. Beginning with the Fourier series for ideal impulses or square waves, we modify the magnitude of each term with a Gaussian roll-off characteristic. For a baseband system using harmonic numbers from 0 through N, each nth harmonic is attenuated by the factor K_n

$$K_n = \exp\left\{-(\ln\sqrt{2})\left(\frac{n}{PN}\right)^2\right\}, \qquad 0 \le n \le N \quad (7)$$

where P is the fractional 3-dB bandwidth, that is, the fraction of the total band for which the attenuation is less than 3 dB. Similarly, for a bandpass case, where harmonic numbers from N_1 to N_2 are used and both lower and higher harmonic frequencies are suppressed, the function chosen is

$$K_n = \exp\left\{-(\ln\sqrt{2})\left(\frac{2n - N_2 - N_1}{PN_2 - PN_1}\right)^2\right\}, \qquad N_1 \le n \le N_2. \quad (8)$$

Evaluating the initial Fourier series coefficients and applying the roll-off function gives the following input coefficients to be used in (6). The factor H normalizes the peak value to 1.0, in cases 1) and 3) of the following.

1) Baseband Impulse:

$$V_{cn} = \frac{1}{H}\exp\left[-(\ln\sqrt{2})\left(\frac{n}{PN}\right)^2\right], \qquad \text{for } 0 \le n \le N$$

$$V_{sn} = 0$$

$$H = \sum_{n=1}^{N} \exp\left\{-(\ln\sqrt{2})\left(\frac{n}{PN}\right)^2\right\} + 0.5.$$

2) Square Wave (Step Function):

$$V_{co} = 1$$

$$V_{cn} = 0, \qquad \text{for } n > 0$$

$$V_{sn} = \frac{2}{n\pi}\exp\left[-(\ln\sqrt{2})\left(\frac{n}{PN}\right)^2\right], \qquad \text{for } n \text{ odd}, 0 < n \le N$$

$$V_{sn} = 0, \qquad \text{for } n \text{ even.}$$

3) For the RF Pulse (Bandpass Network):

$$V_{cn} = 0, \qquad \text{for } n < N_1, n > N_2$$

$$V_{cn} = \frac{1}{H}\exp\left[-(\ln\sqrt{2})\left(\frac{2n - N_2 - N_1}{PN_2 - PN_1}\right)^2\right], \qquad \text{for } N_1 \le n \le N_2$$

$$V_{sn} = 0$$

$$H = \sum_{n=N_1}^{N_2} \exp\left\{-(\ln\sqrt{2})\left(\frac{2n - N_2 - N_1}{PN_2 - PN_1}\right)^2\right\}.$$

Generation of the time-domain response for these cases involves evaluation of the responses of the network, $\hat{S}_n$ and θ_n, for each harmonic, the evaluation of (6) at many closely spaced instants of time sufficient for the graph desired, and plotting the results. The summations in (6) are, of course, limited to the harmonic numbers used in the measurements.

We have commonly used 81 frequency components which may or may not include zero frequency. For example, the fundamental may be 225 MHz, and all multiples up to 18 GHz may then be used, including zero. Alternatively, for the 2–4-GHz band, the fundamental may be 25 MHz, the lowest harmonic number N_1 will be 80, the highest N_2 will be 160, and the center N_c will be 120. In the first case, we can plot over a time range of 4.44 ns corresponding to a round-trip path length of 1.33 m, with a time resolution on the order of 0.05 ns, corresponding to a radar location distance resolution of ~0.75 cm. For narrower bandwidth plots, the available time span is increased and the resolution is degraded in inverse proportion.

Fig. 1 shows four sets of transmission response curves computed with our program for a simple network consisting of a 10-cm length of lossless TEM line. We assumed $\hat{S}_n = 1$, $\theta_n = -20\ \pi n f_1/c$. These curves are accurate replicas of the presumed input waves, delayed 0.33 ns. Without the pulse-shaping filter, we observe excessive ringing and overshoot. The filter degrades the rise time and resolution, but reduces the ringing and overshoot to give a more easily interpreted display, with reduced interference between separate closely spaced responses. The half-height width of the impulse function is 33 ps unfiltered and 48 when filtered. The 10–90-percent rise time of the filtered step response is seen to be ~40 ps and ~25 ps for the unfiltered case.

These curves are mathematical constructions representing hypothetical input wave functions. These hypothetical waves are *totally* band limited to the frequency range of the network measurements with a predetermined, discrete, and finite set of spectral components. Therefore, *the networks' response to these assumed input waves can be accurately determined in detail by these techniques.* The accuracy is limited only by the precision of the network measurements, by roundoff errors of the computer, and by the plotting technique used. However, it must be recognized that the *input* wave is not a *single* impulsive event, but a *rounded* and *periodically repetitive* approximation of one. The time-response curves generated are fully valid with this interpretation. In many cases, the

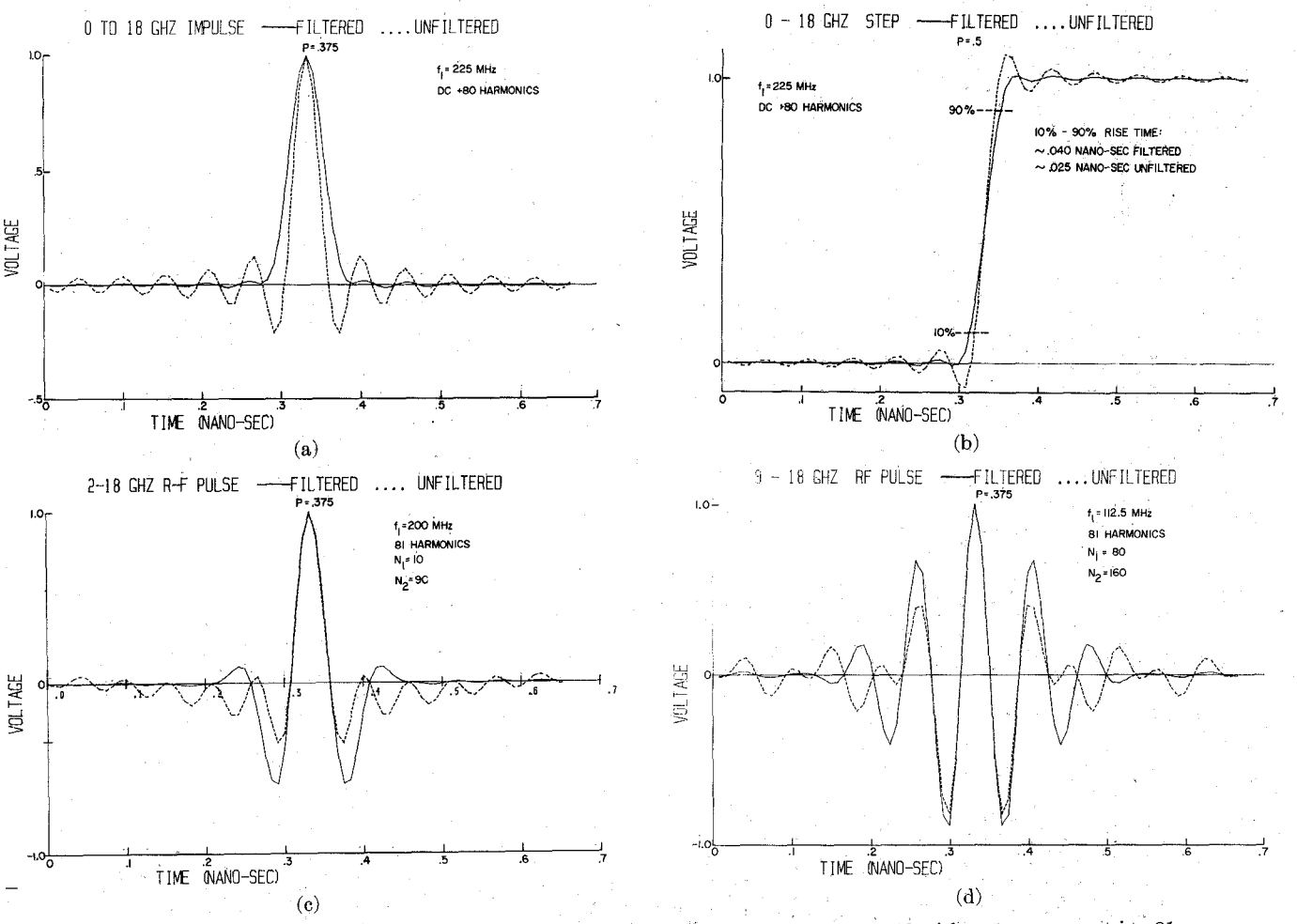

Fig. 1. Time-domain transmission responses for a 10-cm lossless TEM line, computed with our program, using 81 harmonics of the Fourier series, but with theoretical frequency response data, $S_n = \exp(-j2\pi nl/Tc)$, where $l = 10$ cm, $T = 1/F_1$, $c = 3 \times 10^{10}$ cm/s. These are undistorted replicas of four examples of input time-functions, delayed 0.333 ns. Responses of this shape are obtained with simple flat-band gain or loss, and as reflections from resistive discontinuities in TEM lines. The Gaussian filter suppresses the long ringing transients, but degrades the rise time. (a) Impulse response. (b) Step response (rising edge of a square wave). (c) RF pulse for the 2–18-GHz band. (d) RF pulse for the 9–18-GHz band.

results can also be interpreted safely as simulating the response to a *single* pulse of this shape. However, if the network involves transient phenomena with time constants comparable to or larger than the repetition period T, then the results must be interpreted with care. For example, large bypass capacitors or dc return inductors in the network may introduce long exponential transients for single-pulse excitation which will be masked when periodic excitation is used. Similarly, the effects of a high-Q microwave resonance can be suppressed in this technique unless the harmonic frequency components used are sufficiently closely spaced to delineate the response characteristics of this resonance.

When a time-domain oscillographic plot shows distinct and separate responses which can be identified with distinct and separate segments of the network, it is *sometimes* possible to reconstruct a set of frequency-domain data from the time-domain plot for *each* such separable network segment. The technique is approximate and subject to errors where there is significant interaction between these parts. The method is straightforward for reflection analysis. In transmission studies, the method is not usually applicable. The technique involves modification and reinterpretation of (1)–(3).

Here the baseband impulse response $V_o(t)$ is used, eliminating the roll-off filter by setting $P \gg 1$. A new function $V_r(t)$ is defined, $V_r(t) = V_0(t)$ for $T_1 \leq t \leq T_2$, $V_r(t) = 0$ for $-T/2 < t < T_1$, and for $T_2 < t < T/2$, where T_1 and T_2 are the time limits encompassing the reflection response of the network segment being studied.

$$V_r(t) \simeq \frac{V_{co}}{2} + \sum_{n=1}^{N} \left[V_{cn} \cos \frac{2\pi nt}{T} + V_{sn} \sin \frac{2\pi nt}{T} \right] \tag{9}$$

$$V_{cn} \simeq \frac{2H}{T} \int_{T_1}^{T_2} V_r(t) \cos \frac{2\pi nt}{T}\, dt \tag{10}$$

$$V_{sn} \simeq \frac{2H}{T} \int_{T_1}^{T_2} V_r(t) \sin \frac{2\pi nt}{T}\, dt. \tag{11}$$

The frequency responses S_n are

$$S_n = (V_{cn}^2 + V_{sn}^2)^{1/2} \exp\left(j \tan^{-1} \frac{V_{sn}}{V_{cn}} \right) \tag{12}$$

where

$$-\frac{T}{2} \leq T_1 < T_2 \leq \frac{T}{2}.$$

To use these equations, we must *assume* that the time response between T_1 and T_2 is identifiable as coming from a distinct segment of the network, that it is *complete* within the range $T_1 \rightarrow T_2$, and that it has not been modified by other network segments. In the integrations of (10) and (11) we artifically restrict the range of integration to $T_1 \rightarrow T_2$, thereby assuming that the response is zero outside of this range. Errors are introduced because the transients of any such response are not, in general, zero outside of such a restricted range, nor are the transients from other network segments totally negligible within the range of integration. Further error can be introduced if the waveform from the network segment being studied has been distorted in transmission through other segments. The technique is useful in suppressing the interference of a good but not perfect transmission-line transducer between the measuring equipment and the network under study. If may also be used to determine the frequency-domain reflections from a poor input transducer which is followed by interfering reflections from subsequent network segments. No detailed analysis has been made to estimate the magnitude of the errors introduced by transient cutoff effects.

III. Some Illustrative Examples

Fig. 2 shows the time-domain response of the reflections of an input impulse, applied to a 10-cm air line, and a 10-dB pad, followed by a short circuit, all with precision APC-7 connectors. The plot uses centimeters as abscissa rather than time, representing the distance to the point of reflection.

The first reflections in the range 0–3 cm represent residual calibration errors plus the first connector. We see next a reflection ~45 dB down at the next connector pair, at 9–11-cm distance. These are followed by larger reflections −39 dB below the input due to pad imperfections. The large negative peak is the reflection from the short circuit, 20 dB down due to two passages through the pad.

Fig. 3 shows the original frequency-response data and reconstructions of the frequency responses of various segments of this network. Reconstruction from the range 9–30 cm shows the combined effects of the pad and the short. The rapid undulations in the upper band have been eliminated as they were caused by interference with the calibration errors. Still further separation for range 9–12 cm shows the effects of the connector. For the range 16–20 cm, we have the effects of the short circuit, attenuated by the pad, but without the interference of the pad's separate reflections.

Fig. 4 shows several reflection conditions for an adjustable shunt capacitor across the line (HP 874B), at a distance of 9 cm. The capacitance settings are 0.0, 0.02, 0.04, and 0.08 pF, giving various reflection magnitudes. It will be seen that there is an observable reflection even at zero setting, unexplained here. The reflections in the range 16–22 cm are from a 10-dB pad and

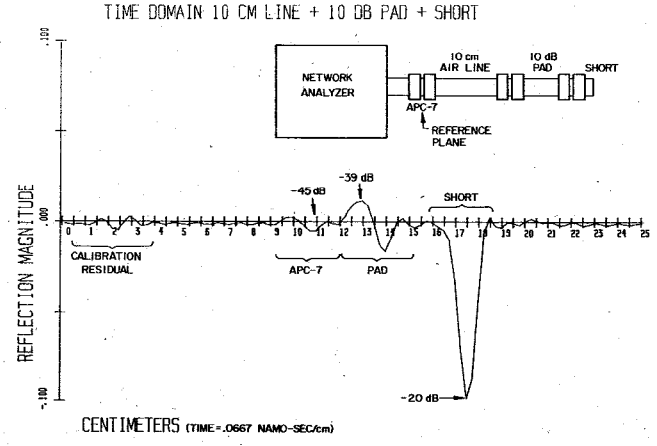

Fig. 2. Time-domain reflectometer response of the network shown, for impulse excitation. Response peaks are unambiguously and quantitatively associated with individual reflection discontinuities as indicated. Abscissa is labeled as centimeters to the point of reflection.

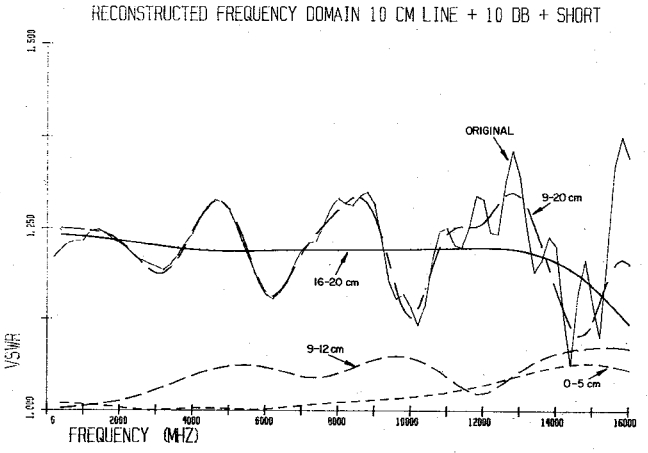

Fig. 3. Original frequency-response data (VSWR) and reconstructed frequency responses from fractional time-period segments of the time-domain responses of Fig. 2. Curves are marked with the centimeter (time) range used for integration by the computer.

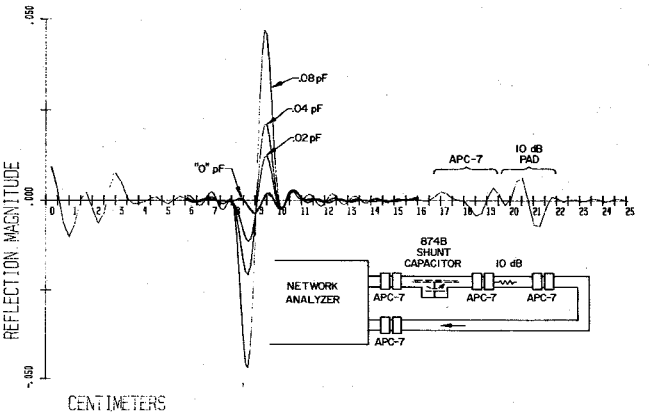

Fig. 4. Time-domain impulse reflections from an adjustable shunt capacitor (HP 874B) across a coaxial line, for 0.0-, 0.02-, 0.04-, and 0.08-pF settings.

its connectors. A frequency-domain reconstruction for the 0.08-pF case is shown in Fig. 5. Here we have eliminated the interference due to the connectors, the pad, and the calibration errors, leaving a smooth, nearly linearly rising characteristic as expected.

Fig. 6 shows the impulse-reflection response of a special test fixture consisting of a 10-cm length of coaxial line, followed by a transducer connecting directly to the open end of a section of ceramic microstrip line of low impedance, estimated to be 10 Ω. The microstrip line was shorted to ground at its far end, and was approximately 4 cm long. The ceramic has a dielectric constant of ~9, giving an apparent electrical length of ~12 cm.

We see here the simulated effect of a short pulse induced on the low-impedance line, reflecting back and forth several times. The input positive pulse is first reflected by the low-impedance mismatch as a negative pulse, at 17-cm distance. A positive pulse is injected into the low-impedance line. It travels to the far (shorted) end and returns as a negative pulse, a part of which escapes back to the source as a second negative pulse at an apparent distance of 29 cm. This pulse is largely reflected again, remaining negative because the microstrip line sees a high-impedance mismatch. This pulse travels again down the line, is inverted again at the short into a positive pulse which again reaches the transducer, allowing a smaller positive pulse to escape at ~41 cm. The process now repeats again and again, inverting the pulse at each reflection from the far end, growing smaller each time as some energy escapes at the input, and some is lost in line attenuation. At 146 cm, the process starts again with a new input pulse.

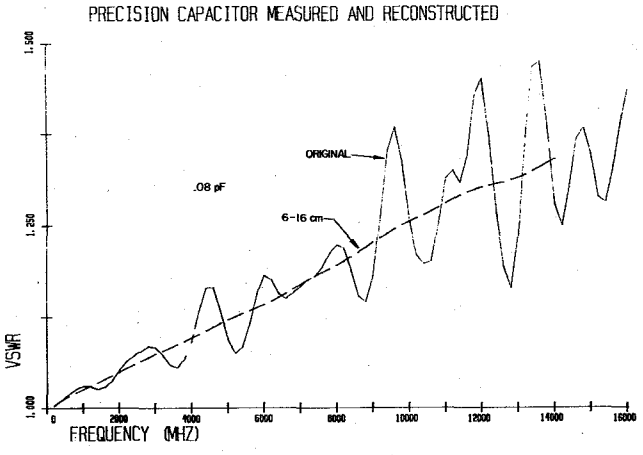

Fig. 5. Frequency-domain data for the 0.08-pF response of Fig. 4, using the range 5.5–16 cm for the limits of integration in reconstruction.

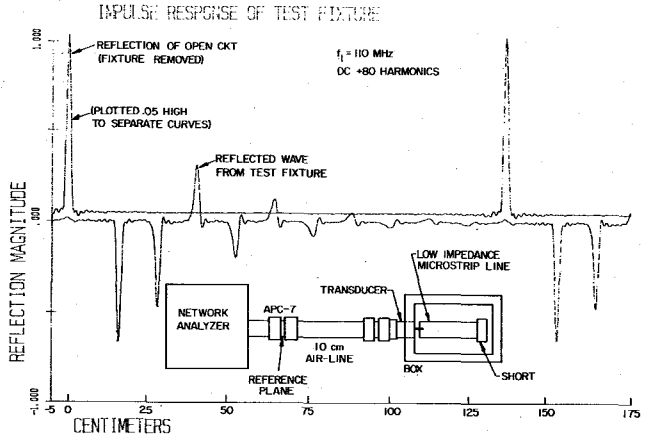

Fig. 6. Impulse-reflection response of a special demonstration test fixture, consisting of 10 cm of coaxial line, a transducer, and a 4-cm length of low-impedance microstrip line, shorted at the far end. Its electrical length is ~12 cm. Multiple reflection peaks appear as the simulated impulse travels back and forth along the microstrip line, releasing a fraction of its energy each time it reaches the transducer. The polarity of the impulse reverses each time it is reflected at the shorted end. The display is periodic, repeating at an apparent electrical distance of ~136 cm (9.09 ns). Also shown is the reflection response of the open-circuited input line when the test fixture was removed. This represents the input wave.

Fig. 7 shows the reflection response of the same fixture to an input square wave. The gross features of this curve may be explained in a manner quite similar to the above. At first glance, this appears to be an inverted and delayed square wave, as expected from a short circuit, with a smaller decaying square-wave transient superposed. The decaying transient is clearly the result of multiple reflections on the low-impedance line. However, there is further fine structure on this curve needing further explanation. In the middle of the range 17–27 cm, for example, there is a small subsidiary step which can be explained as a remnant of the decaying transient from the next previous step-down, one-half of the period earlier. Here we have an example of a network with a time constant comparable to the cycle period T. Here we must not interpret the square-wave response as being equivalent to the step response, even in the periods immediately following the input steps which are applied. However, if we were to use a sufficiently longer period T, with a lower fundamental frequency $f_1 = 1/T$, these overlapping transient effects could be suppressed, allowing a relatively accurate simulation of the step response using the square wave. To retain the same time resolution, however, more harmonics would then be required.

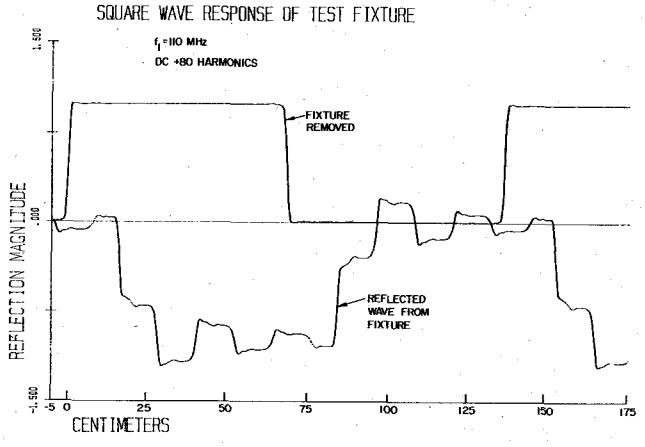

Fig. 7. Square-wave reflection response of the test fixture for Fig. 6, and the response of the input open circuit when the fixture was removed.

IV. Conclusions

Useful oscillographic response plots of a microwave network have been obtained by computer simulation, using frequency-domain data measured with a computer-controlled network analyzer. The technique has a short time resolution, is highly sensitive, and provides quantitative results useful in a variety of ways. A major application is in the analysis of impedance data at the input of transmission networks, where it serves as a quantitatively interpretable time-domain reflectometer. It may also be used to measure small reflection coefficients of individual parts of multiple-section networks, which are physically inseparable both in the time domain and the frequency domain.

References

[1] D. L. Hollway, "The comparison reflectometer," *IEEE Trans. Microwave Theory Tech.*, vol. MTT-15, pp. 250–259, Apr. 1967.
[2] P. I. Somlo, "The locating reflectometer," *IEEE Trans. Microwave Theory Tech.*, vol. MTT-20, pp. 105–112, Feb. 1972.
[3] L. A. Robinson, W. B. Weir, and L. Young, "An RF time-domain reflectometer not in real time," *IEEE Trans. Microwave Theory Tech. (1972 Symposium Issue)*, vol. MTT-20, pp. 855–857, Dec. 1972.
[4] A. M. Nicolson, C. L. Bennett, Jr., D. Lamensdorf, and L. Susman, "Applications of time-domain metrology to the automation of broad-band microwave measurements," *IEEE Trans. Microwave Theory Tech. (Special Issue on Automated Microwave Measurements)*, vol. MTT-20, pp. 3–9, Jan. 1972.

De-Embedding and Unterminating

RONALD F. BAUER, MEMBER, IEEE, AND PAUL PENFIELD, JR., FELLOW, IEEE

Abstract—**De-embedding is the process of deducing the impedance of a device under test from measurements made at a distance, when the electrical properties of the intervening structure are known. Unterminating is the process of deducing the electrical properties of the intervening structure from a series of measurements with known embedded devices. The mathematical steps necessary for de-embedding and unterminating are reviewed, and a technique is presented for unterminating with theoretically redundant measurements in order to minimize the effect of experimental errors.**

I. Introduction

At microwave frequencies it is often impossible to directly measure the impedance (or admittance or reflection coefficient) of devices such as diodes or transistors. Instead, measurements are made at, and referred to, some reference plane physically removed from the device. The device is then said to be "embedded" in the intervening structure. If the device under test is a two-terminal device, then the "embedding network" may usefully be regarded as a two-port network $\mathfrak{N}_E$, with the measurement plane at the input and the device under test terminating the output. This is shown in Fig. 1.

A related problem is that of characterizing, for a working circuit, the region surrounding a device such as a diode. For example, one might wish to know the impedance seen by the diode, or the coupling between the diode and the circuit input or output. It is often impossible to make measurements at the physical location of the device, so what is needed is a characterization of the structure between the device and a convenient measurement plane. Again it is useful to consider the device as "embedded" in the intervening structure, which in the case of a diode may be regarded as a two-port network $\mathfrak{N}_E$. Fig. 1 is again relevant.

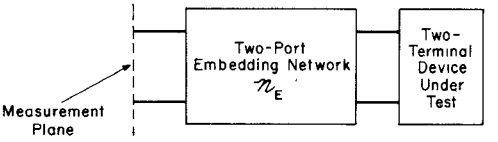

Fig. 1. Normal measurement situation. Characteristics of the device under test can only be measured as they appear outside the embedding network $\mathfrak{N}_E$.

To fix ideas in this paper, we shall consider mainly impedance (instead of admittance or reflection coefficient) measurements, and call the device under test a "diode."

There are two distinct problems. One is, given the measured impedance at the input of the two-port network, to deduce the impedance of the diode. This process, known as "de-embedding," is straightforward, once the embedding network is known, and is discussed in Section II. The other more difficult problem is to characterize the

Manuscript received July 30, 1973; revised October 18, 1973. This work was supported by the Department of the Air Force.
R. F. Bauer is with the M.I.T. Lincoln Laboratory, Lexington, Massachusetts 02173.
P. Penfield, Jr., is a Consultant at the M.I.T. Lincoln Laboratory, Lexington, Massachusetts 02173, and is with the Department of Electrical Engineering and Research Laboratory of Electronics, Massachusetts Institute of Technology, Cambridge, Massachusetts.